Tensile behavior of textile reinforced concrete subjected to freezing–thawing cycles in un-cracked and cracked regimes

Isabella Giorgia Colombo [1], Matteo Colombo [1], Marco di Prisco [1]

Politecnico di Milano, Department of Civil and Environmental Engineering, Piazza Leonardo da Vinci 32, 20133 Milano, Italy

Received 12 June 2014
Accepted 3 March 2015
Available online 29 March 2015

1. Research significance

Durability is a key issue when considering structural material. As textile reinforced concrete can be used by engineers and architects to design thin cross-section structural elements and retrofitting layers, good durability, including in an aggressive environment, is required. The freezing–thawing phenomenon represents a very severe condition to which the material can be subjected. There is a lack of information about TRC in this field. This study represents a starting point from which to understand how the mechanical behavior of TRC, investigated in tension, is affected by exposure to freezing–thawing cycles.

2. Introduction

Textile reinforced concrete (TRC) is a composite cement-based material reinforced with fabrics that allows designers to obtain thin and lightweight structures characterized by a high tensile strength. The ability to orient the reinforcement in the direction of the tensile forces, the bi-axial load capacity and the no concrete cover requirement against corrosion are the main advantages of such composite material. Reinforcing fabrics could be made of carbon, aramid or alkali-resistant glass; the latter reinforcement is the most widely used because of its good strength/cost ratio, even if the alkalinity of the cementitious matrix can affect the mechanical behavior of the composite. Butler et al. [1] observed that the decrease in toughness with increasing alka-linity depends mainly on the formation of solid phases in the fabric–matrix interface, rather than on deterioration of the AR glass fabric.

The fields of application of this composite material include both new structures and existing buildings [2,3], and, in particular, facade panels, precast multi-layered roof and wall panels, tunnel linings, and the retrofitting of damaged structural elements.

As TRC is a structural material, its durability must be proved in order to guarantee maintenance of the mechanical response during the expected life time of the construction.

Several researchers have developed durability models to quantify strength loss in textile reinforced composites resulting from AR-glass degradation problems and weathering conditions (humidity and temperature) [4,5]. Others have focused on the effect of matrix composition (hydration kinetics and alkalinity) on TRC durability [1], observing that an alkali reduced matrix demonstrates strong performance even when exposed to accelerated ageing.

When a TRC layer is exposed to an external environment, it may be the subject of freezing–thawing attacks, and its durability can be reduced.

Some codes, such as ASTM C666 [6], present methods to evaluate freezing–thawing durability, but the main aim of these standards is to compare different concrete mixes and not to quantify the expected service life due to material performance. In fact, as underlined by Neville [7], it is difficult to define a correlation between the number of cycles performed in the lab and the service life of actual concrete because it is difficult to determine the number of cycles to which an element is exposed, especially in a south-facing exposure. *However, the ability of concrete to withstand a considerable number of laboratory freezing and*

E-mail addresses: isabellagiorgia.colombo@polimi.it (I.G. Colombo), matteo.colombo@ polimi.it (M. Colombo), marco.diprisco@polimi.it (M. di Prisco).
URL's:URL:E-mail addresses:E-mail address: http://www.dica.polimi.it (I.G. Colombo), http://www.dica.polimi.it (M. Colombo), http://www.dica.polimi.it (M. di Prisco).
[1] Tel.: +39 02 2399 8790; fax: +39 02 2399 8771.

Table 1
Mix design w/(c + s) = 0.19.

Component	Content
Cement I 52.5	600 kg/m^3
Sand 0–600 μm	957 kg/m^3
Water	209 l/m^3
Superplasticizer	56 kg/m^3
Slag	500 kg/m^3

thawing cycles (say 150) is a probable indication of its high degree of durability under service conditions [7].

According to Neville [7], freezing–thawing damage in concrete occurs when the dilating pressure due to the freezing of water in the cap-illary pores exceeds the tensile strength of the material. This expansion causes an increase in the volume of water of about 9%, and the conse-quent expulsion of excess water; the pressure depends on the resistance to flow, related mainly to the permeability of the hardened cement paste (the higher the permeability the lower the pressure). An increase in total moisture content due to the diffusion of water during thawing caused by osmotic pressure magnifies the phenomenon. The repetition of freezing–thawing cycles leads to the development of pressure and its consequences.

The resistance of concrete to freezing–thawing phenomena depends on the degree of saturation, the pore system of the hardened cement paste (distance to the nearest unfilled void), permeability and the water to cement ratio.

If the degree of saturation in the concrete is below a certain thresh-old, the material is highly resistant to frost (dry concrete is totally unaf-fected). The critical saturation of concrete depends on the size of the body, its homogeneity and the rate of freezing. If excess water can be ex-pelled into cavities closed enough to the pores in which ice is being formed, the material is characterized by having no critical saturation value. In conventional concrete, the use of a proper amount of air entrained agent (AEA) is essential because air bubbles created in the paste can shorten the water paths and provide additional space for the escape of excess water, preventing the development of dilating pressure [8].

Low permeability and a low water/binder ratio are other two fundamental properties that characterize concrete with high freezing–thawing resistance. High strength concrete (HSC), typically characterized by a water to binder ratio lower than 0.30 and by a very low permeability, is considerably less vulnerable to freezing–thawing attack than conventional concrete [9 and 10, considering up to 500 and 700 cycles respectively], even without using AEA [8]. This is due to the fact that, on one side, a limited amount of water can penetrate the con-crete and, on the other side, the pores in HSC are very fine and it is difficult for pore water to freeze. It is still not clear whether the use of AEA is necessary in the case of HSC to make it freezing–thawing

Table 2
Characteristics of the fabric.

Material	AR-glass
Coating	Water resin based on styrene–butadiene rubber (SBR)
Fabrication technique	Leno weave
Warp yarn spacing [mm]	4.9
Weft yarn spacing [mm]	10.1
Warp [Tex]	2 × 1200
Weft [Tex]	1200
Warp filament diameter [μm]	19
Weft filament diameter [μm]	19
Coating weight [g/m$^2_{fabric}$]	100
Maximum tensile load on 70 mm [kN][a]	11.02

[a] Average values of 10 tensile tests.

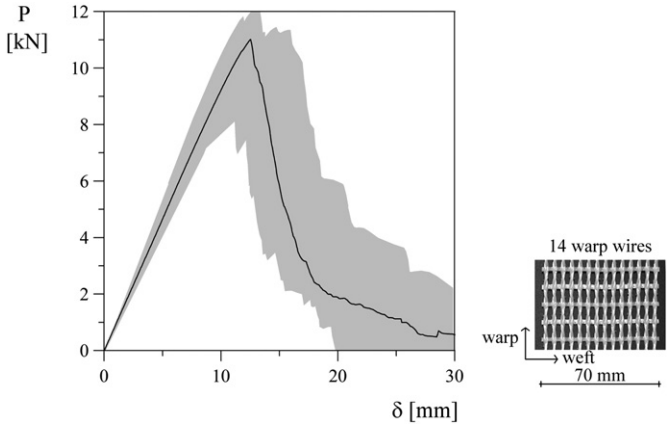

Fig. 1. Uniaxial tensile behavior of the fabric along warp direction: load vs. displacement average curve and fabric geometry [17].

resistant [11]: controversial results were obtained in this respect, as summarized by Wang et al. [12] who explained it through the deficiency of standard test methods and differences in the mixing and curing methods adopted. Experience has shown, however, that the criteria adopted to classify conventional concrete as freezing–thawing resistant (e.g. those proposed by Canadian Standard CSA A23.1 [13]) are too se-vere in the case of HSC [11].

Load combined with the action of freezing and thawing considerably reduces the number of cycles before failure for both conventional and high strength concrete: the lower the grade of concrete, the lower the number of cycles sustained [9].

Among cement based composites, few investigations of freezing–thawing behavior can be found for fiber reinforced concrete [14,15], and no information is available for the mechanical performances of TRC in such conditions. As already discussed, freezing and thawing can affect the cement paste and therefore the bond between fabric and mor-tar, that is the main mechanism governing the tensile behavior of TRC. This paper presents the results of experimental research aimed at un-derstanding the deterioration of the tensile behavior of this material when subjected to freezing–thawing cycles.

3. Experimental program

In order to investigate the residual tensile behavior of textile reinforced concrete when subjected to freezing–thawing cycles, a proper experimental program was carried out. The specimens tested were cre-ated by reinforcing a high strength mortar with one layer of AR glass fabric. This section describes the materials involved in the casting proce-dure, specimen preparation (including thermal treatment), test set-up and the test procedure adopted.

3.1. Cementitious matrix

The matrix of the TRC investigated was high strength mortar charac-terized by a water to binder ratio equal to 0.19. Quartzite aggregates were used. The maximum aggregate size was equal to 600 μm in order to allow the matrix to flow through the fabric mesh and, thus, to obtain a good bond between fabric and matrix. The mix design is summarized in Table 1.

The mechanical properties of the matrix were quantified via bending and compressive tests according to the EN 196-1 Standard for mortar [16]. The average bending tensile strength (f_{ctf}) was 13.6 MPa (STD 12.62% on eight nominally identical specimens), and the average cubic compressive strength (f_{cc}) was 97.5 MPa (STD 7.73% on sixteen nomi-nally identical specimens) [17].

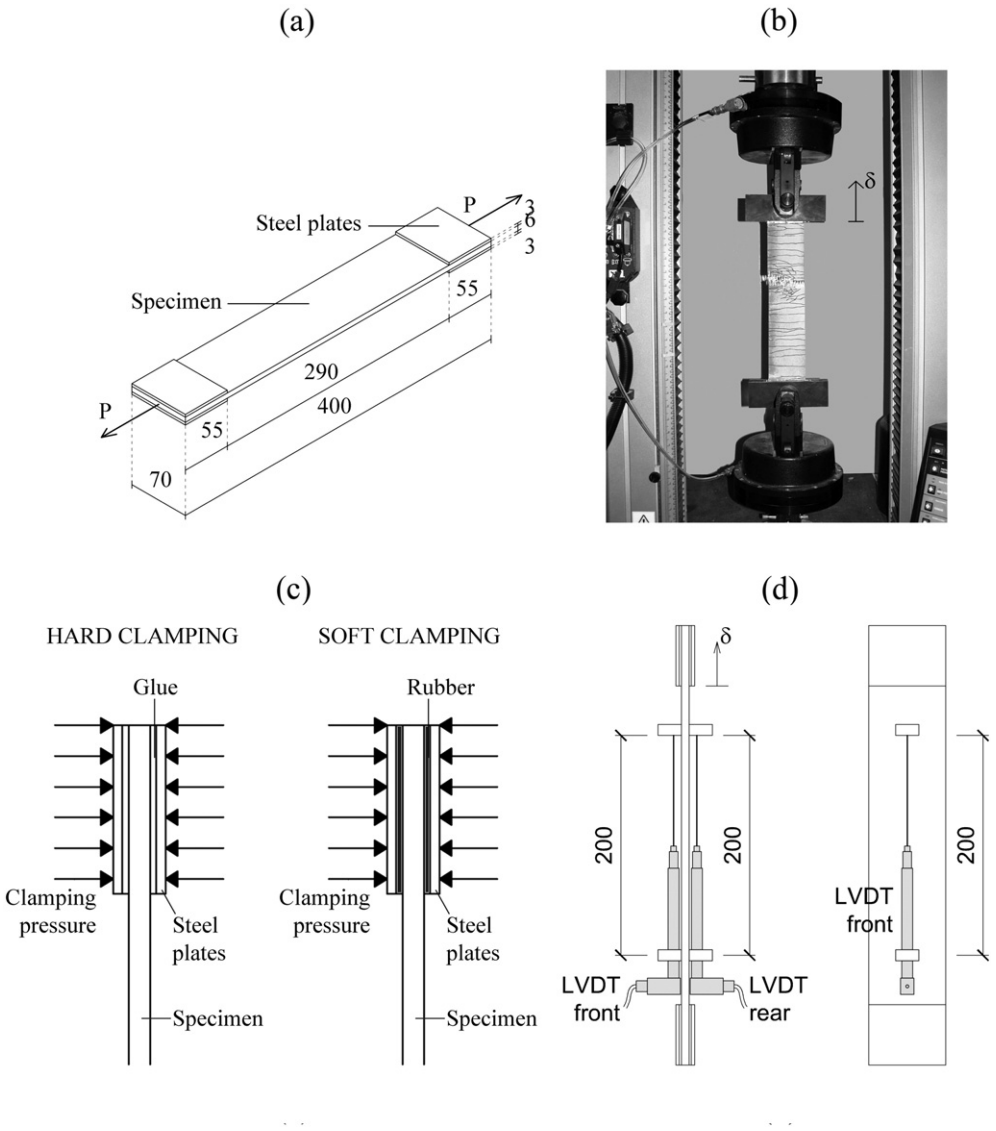

Fig. 2. Specimen geometry (a), tensile test set-up (b), hard and soft clamping system (c), and LVDTs location used in the case C0 (d). Measures in mm.

3.2. AR glass fabric

The fabric used was chosen after a proper investigation (confined to AR-glass fabrics) aimed at optimizing the performance of the composite material in terms of ductility, the bond between matrix and fabric, and the internal filaments slip [17]. The characteristics of the fabric are summarized in Table 2. Ten uniaxial tensile tests were performed on 400×70 mm^2 fabric specimens in order to characterise the fabric tensile behavior. The nominal strength obtained in the warp direction was equal to 820 MPa (evaluated considering the glass filament area as a cross section). Further information on the testing procedure and some discussion of the results can be found in Colombo et al. [17]. The

Table 3
Specimen history: dates of casting, pre-cracking, beginning and end of cycles and performing of the tests.

Specimens	Casting	Pre-cracking	Beginning of cycles	End of cycles	Tension test
U0_1; U0_2; U0_3	30/06/2011	–	–	–	17/01/2012
U25_1; U25_2; U25_3	18/07/2011	–	23/09/2011	28/09/2011	16/01/2012
U50_1; U50_2; U50_3	18/07/2011	–	23/09/2011	04/10/2011	16/01/2012
U75_1; U75_2; U75_3	18/07/2011	–	23/09/2011	10/10/2011	16/01/2012
U100_1; U100_2; U100_3	20/07/2011	–	23/09/2011	15/10/2011	17/01/2012
U150_1; U150_2; U150_3	17/04/2012	–	23/10/2012	24/11/2012	20/12/2012
U500_1; U500_2; U500_3	17/04/2012	–	28/06/2012	05/12/2012	20/12/2012
C0_1; C0_2; C0_3	20/03/2013	21/05/2012	–	–	06/05/2013
C25_1; C25_2; C25_3	12/04/2012	21/05/2012	16/07/2012	21/07/2012	27/07/2012
C50_1; C50_2; C50_3	10/04/2012	21/05/2012	27/09/2012	08/10/2012	26/10/2012
C75_1; C75_2; C75_3	10/04/2012	21/05/2012	28/06/2012	14/07/2012	16/07/2012
C100_1; C100_2; C100_3	10/04/2012	21/05/2012	28/06/2012	21/07/2012	27/07/2012
C150_1; C150_2; C150_3	12/04/2012	21/05/2012	30/07/2012	30/08/2012	24/09/2012
C500_1; C500_2; C500_3	12/04/2012	21/05/2012	28/06/2012	05/12/2012	20/12/2012

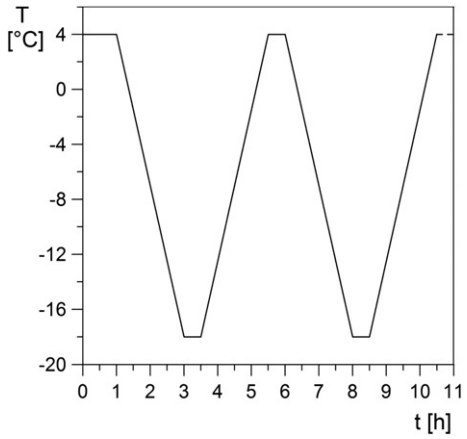

Fig. 3. Freezing–thawing cycles: temperature–time curve.

Fig. 5. Damage to the mortar surface in pre-cracked 500 cycles specimen.

results in terms of load vs. displacement are displayed in Fig. 1, together with a picture representing the fabric geometry. The solid line repre-sents the average curve of ten nominally identical tests, and the shadow represents the area between the minimum and maximum load values measured for each displacement value. An average maximum tensile load equal to 11.02 kN was measured (STD 6.52%) when 70 mm wide specimens were tested.

3.3. Composite preparation

The specimens used in the experimental investigation were 400 mm long, 70 mm wide (b) and 6 mm thick (t) and were characterized by a nominal reinforcement ratio (A_{fabric}/bt) equal to 3.2% (Fig. 2a).

An hand lay-up technique was employed to produce the specimens. A formwork with a transparent bottom plate was used in order to visu-ally check the penetration of the matrix into the fabric mesh. Overlap-ping steel rails (3 mm thick) were designed in order to place the textile layer in the mid-plane of the specimen. Once the first layer of concrete was spread onto the formwork bottom plate and smoothed with a roller, the reinforcement fabric was positioned and fixed, and then the specimen was completed by filling the formwork with another layer of concrete, which was also smoothed. The use of the roller allowed the removal of any air bubbles that could constitute a defect in the matrix. In all the specimens produced the warp was taken parallel to the long side. The specimens remained in the mould for 1 day in a wet environment (>95% RH), and were then cured in air for 28 days before thermal treatment. The environment was that of an office with temperatures ranging between 18 and 22 °C in the winter and between 22 and 27 °C during the summer; the relative humidity ranges were respective-ly 40–60% and 50–80%. Table 3 summarizes the dates related to the specimen history (specimen identification is explained in the following subsection). Previous tests [17] on the same material showed that curing in air guarantees a good mechanical response with respect to other curing conditions; air curing was observed to improve the bond between the matrix and the fabric due to shrinkage. The lack of cracks formed during curing was also due to the fact that the fabric was not constrained at its edges and was free to move together with the mortar.

Even if all surfaces of the specimens were exposed to the air during curing, the shrinkage of the mortar caused a loss of planarity in some specimens. This may be due to a deformability of the fabric that causes, during casting, a small eccentricity of the fabric inside the specimen, thus precluding the perfect symmetry of the specimen itself. The consequent lack of planarity in the specimens was computed by measuring the out-of-plane distance between the two ends of each specimen.

3.4. Thermal treatment

After 28 days in the air, the specimens were sawn and reduced to a length of 375 mm in order to prevent water absorption at the ends of the specimen. In fact, due to the formwork adopted, the fabric overhung the mortar by few centimetres at each end. The specimens were then thermally subjected to different numbers of freezing–thawing cycles according to Procedure A of the ASTM C 666 recommendation [6].The range of temperature varied between +4 °C and −18 °C, with a cooling and heating rate both equal to 11 °C/h, and a 30 min rest phase at both +4 °C and at −18 °C (Fig. 3). Each specimen was completely surrounded by a 2 mm water layer, icing and de-icing during thermal cycles. Different scenarios were considered and, in particular, 25, 50, 75, 100, 150 and 500 cycles were taken into account. Fig. 4 shows the distribution of the specimens in the climatic chamber. In order to take into account the effect of freezing and thawing when the material, even at the Serviceability Limit State, is working in a cracked condition, some specimens were pre-cracked before the thermal cycles.

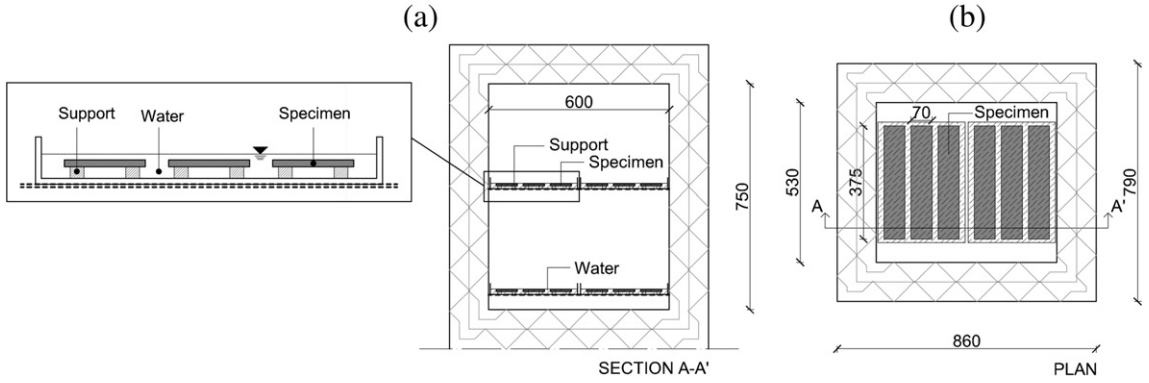

Fig. 4. Freezing–thawing cycles: placement of the specimens in the climatic chamber in section (a) and plan (b) view.

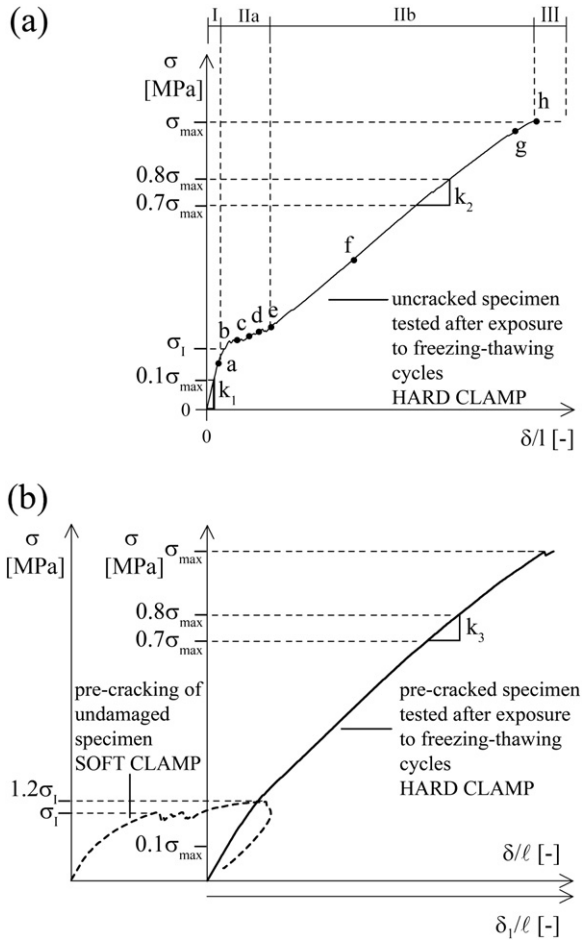

Fig. 6. Test procedure for (a) un-cracked (U), and (b) pre-cracked (C) specimen.

Specifically, three un-cracked and three pre-cracked nominally identical specimens were adopted for each number of cycles considered.

Surface damage was experienced by some specimens after a high number of cycles. In the case of un-cracked specimens, loss of some mortar from the lateral surface was observed after 150 cycles, and after 500 cycles a light deterioration of the upper surface was visible. The phenomenon was more evident in the pre-cracked specimens:

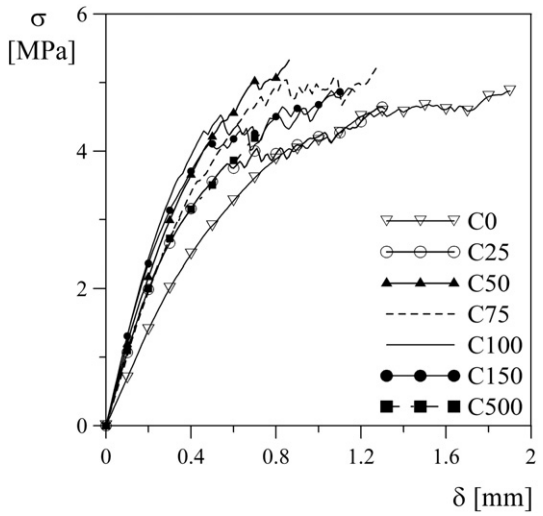

Fig. 7. Pre-cracking. Nominal stress vs. displacement average curves in uniaxial tension.

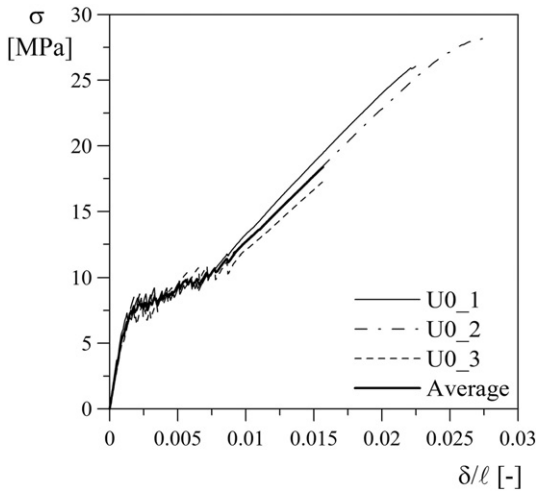

Fig. 8. Un-cracked 0 cycle specimens. Nominal stress vs. normalized displacement curves in uniaxial tension.

damage to the upper surface was demonstrated from 75 cycles and grew with an increasing number of cycles (Fig. 5). This deterioration caused a loss of specimen mass that must be regarded when mass var-iation due to cycle exposure is analyzed. It is worth noting that the sur-face damage was only to the upper surface, which was not in contact with the formwork, while the lower surface was always in perfect con-dition. This must be taken into account in design of the production pro-cess of a structural product.

Once exposed to thermal cycles, each specimen was tested under uniaxial tension according to the experimental set-up described in the following. The same test set-up was used to pre-crack the specimens. Three nominally identical specimens, not thermally damaged, were used as a reference for the mechanical properties.

Each specimen is identified through the following notation: a letter, which specifies whether the specimen was un-cracked (U) or pre-cracked (C) when thermally treated; a number, which stands for the number of cycles to which the specimen was exposed, and another number that denotes nominally identical specimens (e.g. U500_2 stands for un-cracked specimen treated through 500 cycles, specimen number 2).

3.5. Uniaxial tension test procedure

The uniaxial tensile tests were carried out using an INSTRON 5867 electromechanical press with a maximum load capacity of 30 kN. A pressure equal to 5.1 MPa was applied to clamp the specimen edges according to a hard clamping scheme (Fig. 2c) for which $55 \times 70 \times 3$ mm^3 steel plates were glued on each face of the specimen ends in order to better distribute the clamping pressure and thus mini-mise the damage associated with the local crushing of concrete. Backlashing the clamping devices prevented torsional and bending mo-ments caused by an eventual misalignment of the constraints. The tests were displacement-controlled by imposing a constant stroke (δ in Fig. 2b) rate equal to 0.02 mm/s. The test set-up is shown in Fig. 2b.

The pre-cracking phase was carried out with the same test set-up explained above, but using a soft clamping system (Fig. 2c): in this sys-tem, the plates adopted to minimise the local crushing of concrete were not glued, only supported by the clamping pressure applied by the press; a thin rubber interlayer was placed between the specimen and each steel plate to prevent local stress concentration caused by the un-even concrete surface. In this case, as explained by Hartig et al. [18],the load transfer is based on the Coulomb friction, and cracks can occur in the supported parts of the specimen. As slip occurred between specimen and clamping devices, larger displacements were recorded when

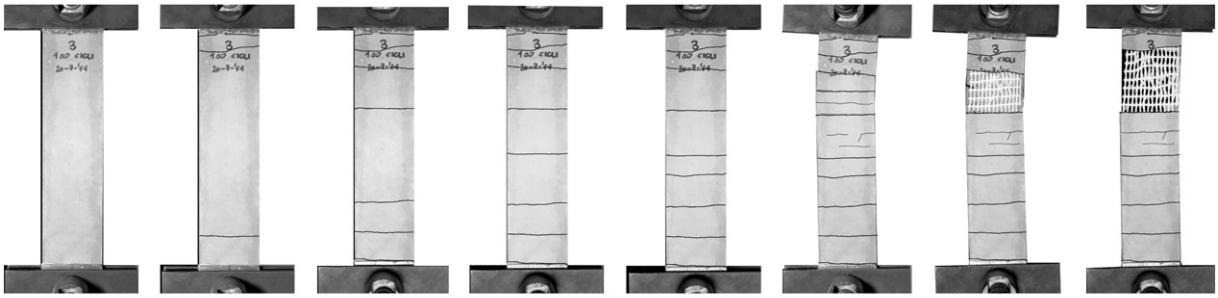

Fig. 9. Typical sequence of crack patterns during a test (each point is indicatively identified in the σ-δ/l curve of Fig. 6a; specimen U100_3 is taken as an example).

compared with the hard clamping case, so the stiffness of the initial elastic branch is smaller.

Fig. 6 describes the test procedure adopted for un-cracked (6a) and cracked (6b) specimens. The un-cracked specimens were exposed to thermal cycles and then tested under direct tension up to failure with hard clamping. Conversely, in the case of cracked situation, the speci-mens were pre-cracked under uniaxial tension via the soft clamping scheme up to a load corresponding to 1.2 times the first cracking load of the specimen itself (dashed curve in Fig. 6b). Once pre-cracked, each specimen was exposed to thermal cycles and then tested under uniaxial tension up to failure with hard clamping (solid curve in Fig. 6b). Two displacement references are also introduced in Fig. 6b: in particular, δ refers to the displacement from the pristine condition (be-fore pre-cracking), and δ_1 was measured from the end of the pre-cracking phase.

The load introduction length used for the tensile tests may cause, in this region, some sliding within the textile that, in any case, did not pre-vent the multi-localization phenomenon and might not affect the max-imum load in a significant way. However, in the case in which freezing and thawing affects bond, an influence of this introduction length on the maximum load can be expected. In any case, at the peak load, the fabric failed in all the tests and not too close to the clamped ends. The sliding occurrence implied that strain values could not be considered reliable as absolute values; because of this the authors decided to consider the value of normalized displacement only in the sense of comparison be-tween different thermal treatments. Such a comparison is not affected by the sliding because all tests have been performed according to the same boundary conditions.

4. Experimental results

4.1. Pre-cracking phase

Fig. 7 shows the nominal stress ($\sigma = P/A$; P = load, A = original cross-section area) versus displacement (δ) curves obtained during the pre-cracking operation for all specimens. Each curve represents the average of three nominally identical tests. It is worth noting that each average curve in the graph, and in all following graphs, is interrupted when the first of the three nominally identical specimens reaches the ultimate displacement; as a result, the peak of the average curve differs from the average peak value. It should be remembered that all pre-cracking operations were performed before the thermal cy-cles and, therefore, the curves presented in Fig. 7 do not refer to the thermally damaged material. The number of cycles displayed in the leg-end refers simply to the cycles to which the specimen will be exposed after the pre-cracking phase. The scattering of the results is due to the soft clamping system, which enhances the slip of the specimen in the clamped zone.

4.2. Uniaxial tension test results

The results of the experimental campaign are reported in this paragraph in terms of nominal stress (σ) vs. normalized displacement (δ/l) curves. The stress is obtained by dividing the load by the initial area of the specimen's cross section; the normalized displacement was evaluat-ed as the ratio between the displacement (δ, Fig. 2b) and the specimen's initial free length (l).

Table 4
Tensile test results—un-cracked (U) specimens.

		t [mm]	b [mm]	$\Delta m/m_i$ [%]	P_{max} [kN]	δ_u [mm]	σ_{max} [MPa]	δ_u/l [%]	σ_l [MPa]	EF [−]
U0 (batch 1)	Average	6.2	70.6	–	11.57	7.19	27.13	2.50	6.10	1.05
	Scattering	3.2%	0.1%	–	4.8%	10.0%	4.0%	10.0%	19.8%	0.5%
U25 (batch 2)	Average	6.0	70.6	0.15%	11.90	7.04	27.94	2.71	8.34	1.08
	Scattering	2.8%	0.6%	73.3%	1.8%	8.0%	1.3%	10.0%	17.5%	1.9%
U50 (batch 2)	Average	6.0	70.7	0.38%	11.02	7.00	25.95	2.64	6.63	1.00
	Scattering	0.0%	1.6%	13.2%	2.9%	8.6%	3.3%	6.8%	28.2%	3.0%
U75 (batch 2)	Average	6.2	70.4	0.82%	11.68	6.74	26.60	2.58	7.71	1.06
	Scattering	1.6%	0.9%	3.7%	6.0%	8.5%	5.0%	8.5%	9.5%	5.7%
U100 (batch 5)	Average	6.2	70.2	1.44%	10.58	6.29	24.20	2.39	9.67	0.96
	Scattering	4.8%	0.4%	6.2%	1.4%	4.0%	5.2%	3.8%	11.8%	1.0%
U150 (batch 6)	Average	6.4	70.4	3.26%	10.53	6.79	23.22	2.48	4.01	0.95
	Scattering	3.1%	0.4%	12.6%	5.4%	8.7%	3.3%	8.5%	14.2%	5.3%
U500 (batch 6)	Average	5.9	70.5	3.33%	9.19	5.99	21.96	2.18	4.42	0.83
	Scattering	1.7%	0.6%	6.6%	6.3%	7.2%	7.1%	7.3%	41.2%	6.0%

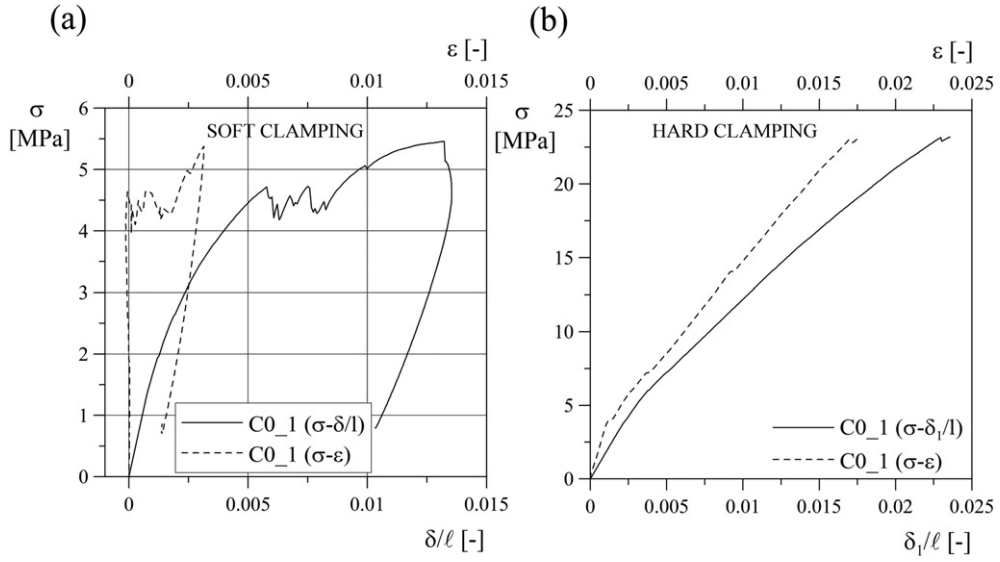

Fig. 10. Pre-cracked 0 cycles—specimen 1. Nominal stress vs. normalized displacement curves in uniaxial tension: pre-cracking phase performed using a soft clamping system (a) and test performed on pre-cracked specimen according to a hard clamping system (b).

Fig. 8 shows the results of the uniaxial tensile tests performed on material not exposed to any thermal cycle (0 cycles, un-cracked). These results were considered as the reference against which to evalu-ate the effect of freezing and thawing on material behavior under un-cracked conditions. In these results the three branches that typically characterize the non-linear response of textile reinforced concrete can be observed (see Fig. 6a: I. First linear branch; IIa. Multi-crack forma-tion; IIb. Crack widening; III. AR glass fabric failure). First cracking was reached when the tensile strength of the matrix was exceeded and then multi-cracking strain hardening behavior occurred. The final branch, in which no further cracks develop, took place: its extension depended on the reinforcement ratio, fabric geometry and coating, and it stopped with fabric failure. A typical sequence of crack pattern evolution during a tensile test is shown in Fig. 9 (as an example pictures concerning specimen U100_3 are shown in the figure); each point (a–h) is indicatively identified on the typical TRC response previously shown in Fig. 6a. The spalling phenomenon only observable in the very final phase of the test (Points g and h) may be due to the small thickness of the specimen with respect to the reinforcing fabric adopted. The only exception to the described behavior is Test U0_3: during this test a transverse crack occurred in the thickness of the specimen within the clamped area, thus causing a slip of the fabric inside the specimen, lead-ing to an earlier failure (Fig. 8). These results are summarized in Table 4, together with those of all the other tests performed on un-cracked ma-terial after exposure to thermal cycles. For each number of cycles per-formed, the table collects the average values and the scatterings of the following parameters, obtained considering three nominally identical specimens in each case:

- the geometrical sizes (thickness t and width b) used to determine the area (A) of each specimen cross-section;
- the percentage variation of the mass after exposure to the thermal cycles ($\Delta m/m_i$; Δm = difference between the final and the initial mass, m_i = initial mass);
- the maximum load reached (P_{max}) together with the corresponding elongation recorded by the machine (δ_u);
- the maximum nominal stress (σ_{max}) together with the correspond-ing normalized displacement ($\delta_{u/}l$);

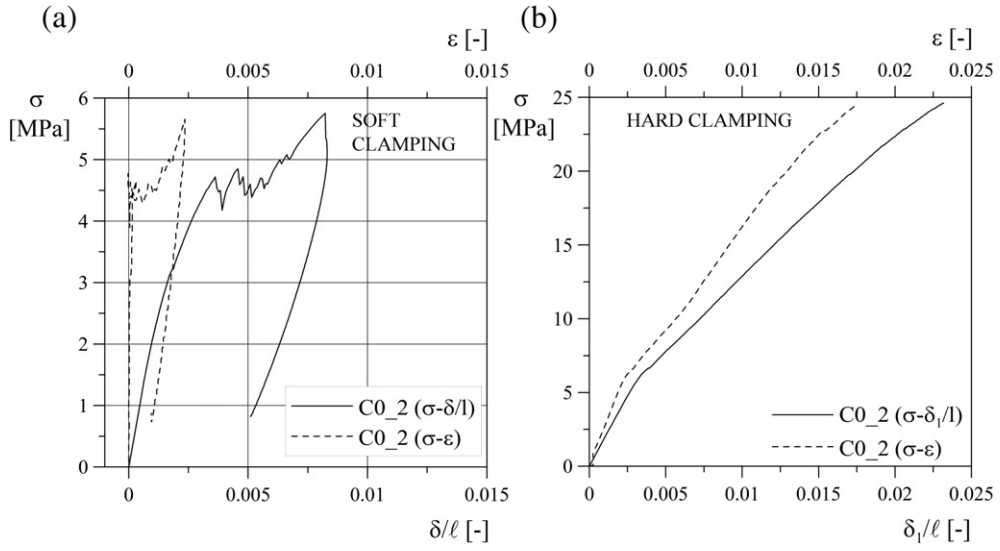

Fig. 11. Pre-cracked 0 cycles —specimen 2. Nominal stress vs. normalized displacement curves in uniaxial tension: pre-cracking phase performed using a soft clamping system (a) and test performed on pre-cracked specimen according to a hard clamping system (b).

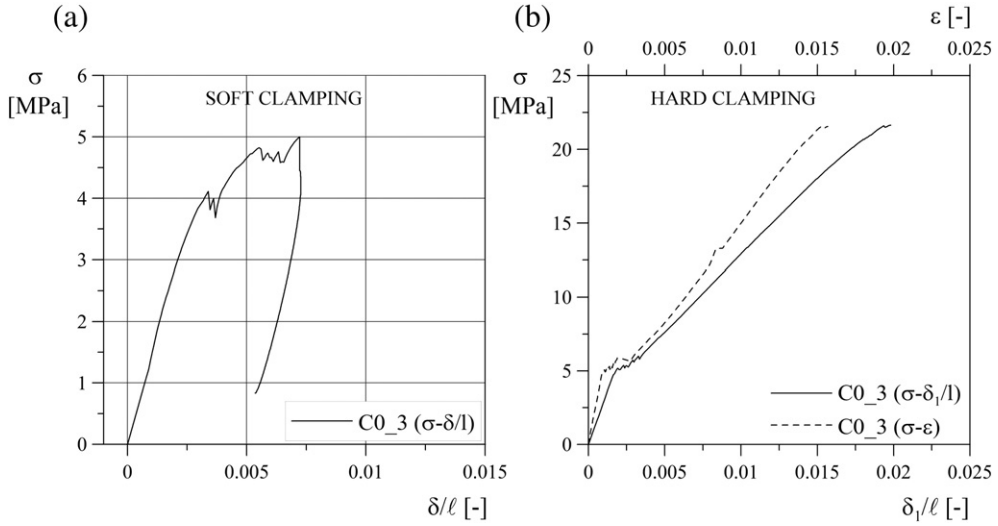

Fig. 12. Pre-cracked 0 cycles—specimen 3. Nominal stress vs. normalized displacement curves in uniaxial tension: pre-cracking phase performed using a soft clamping system (a) and test performed on pre-cracked specimen according to a hard clamping system (b). "C0_3 (σ-ε) pre-cracking curve" is not available in subfigure (a) because of a technical problem in the data acquisition system.

- the first cracking strength (σ_I), obtained, dividing the load corresponding to the first cracking by the initial area of the specimen cross-section (this first cracking load was detected at the point at which the curve deviated more than 2% from the initial stiffness);
- the efficiency factor (EF), calculated as the ratio between the maximum load reached (P_{max}) and the average peak load experimentally measured by stretching the fabric only (Table 2, Fig. 1).

A number, that identifies the batch, is also specified for each group of nominally identical specimens collected in the table. The scattering is computed as the maximum difference between each value and the av-erage one and it is computed as a percentage of the average value.

Three untreated specimens were also tested following the "pre-cracked" test procedure, with soft clamping in the initial phase, up to a certain level of load (1.2 times the first cracking load) and with hard clamping up to failure (Figs. 10, 11 and 12). The average curve obtained is considered the reference for all the pre-cracked specimens tested after exposure to freezing and thawing.

When comparing the results obtained for untreated specimens with the two test procedures in terms of nominal stress versus normalized displacement (σ-δ/l), it is clear that the slip of the specimen inside the clamping region due to soft clamping system affects the first cracking strength (about 30% less than hard clamping). A less significant change (15%) is observable also in the peak strength even if the last phase of the two testing modalities involves the same hard clamping condition.

To better understand the magnitude of the slipping phenomenon, particularly in the soft clamping case, the zero cycle specimens were instrumented with two LVDT displacement transducers, one on the front and one on the rear, during the tests (Fig. 2d). The gauge length astride the centre of each specimen (l_{LVDT}) was equal to 200 mm. In only one pre-cracking phase (C0_3) the LVDT measures were not available due to a technical problem in the data acquisition system (Fig. 12a). The comparison between the nominal strain ($\varepsilon = \delta_{LVDT} / l_{LVDT}$; average between the front and rear values), obtained from the LVDT measures (δ_{LVDT}), and the normalized displacement (δ/l) is shown in Figs. 10, 11 and 12. Subfigure (a) refers to the soft-clamping phase, and subfigure (b) refers to the hard-clamping phase. It is worth noting that the difference between the solid and dashed curves is due to the specimen sliding inside the clamping system. It is quite clear that soft clamping is characterized by greater sliding, and a difference between the two measurements (ε and δ/l), larger than 220%, is seen at the end of the pre-

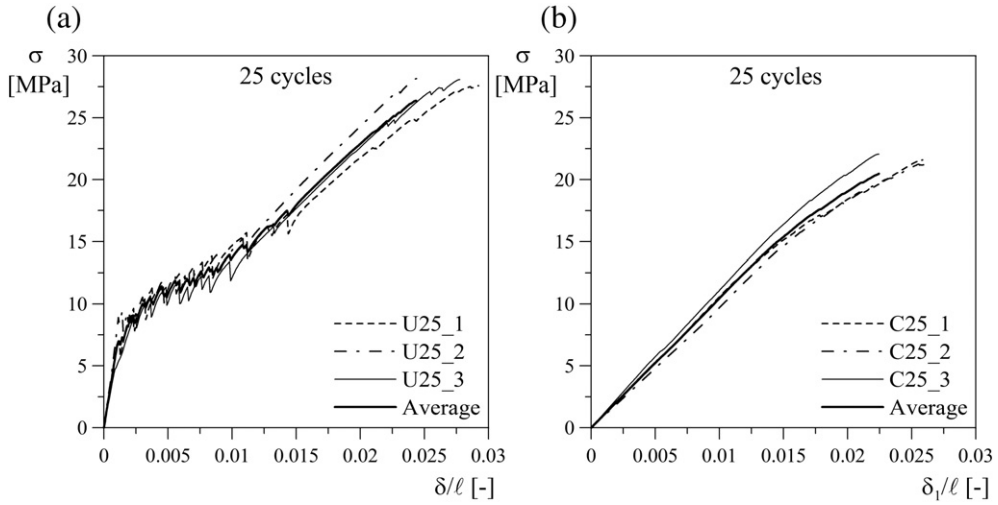

Fig. 13. Twenty-five cycles. Nominal stress vs. normalized displacement curves in uniaxial tension: un-cracked (a) and pre-cracked (b) specimens.

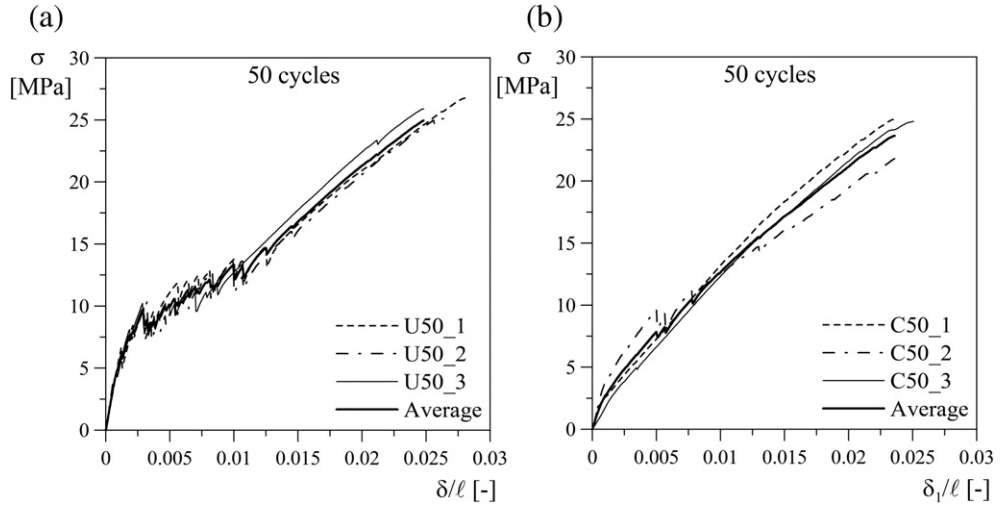

Fig. 14. Fifty cycles. Nominal stress vs. normalized displacement curves in uniaxial tension: un-cracked (a) and pre-cracked (b) specimens.

cracking branch for soft-clamp, while a difference of about 25–30% can be measured at failure for hard-clamp.

The results of the uniaxial tensile tests on the material exposed to several freezing–thawing cycles are presented in Figs. 13–18 respective-ly for 25, 50, 75, 100, 150 and 500 cycles. Subfigure (a) refers to the un-cracked situation, while subfigure (b) involves the pre-cracked speci-mens. In each case, the three curves corresponding to three nominally identical tests are reported, together with the average curve. It is worth noting that the material response is characterized by good re-peatability, even when increasing the number of cycles. There is a slight-ly larger scattering when testing the material exposed to freezing and thawing in cracked conditions, even if a maximum difference between the single and average value of less than 10.5% for the peak load was registered. The same results are summarized in Tables 4 and 5 for un-cracked and cracked conditions respectively.

A comparison between the average curves obtained for all the cycle numbers considered is reported in Figs. 19 and 20 respectively for un-cracked and cracked situations. A typical crack pattern observed at the failure is also presented for each situation in the same figures. It is possible to see that the multi-cracking pattern is denser in the case of pre-cracked specimens, when compared with un-cracked specimens.

A general look at the average curve comparison suggests that freez-ing and thawing has a negligible effect on the ultimate strength of the composite in both un-cracked and cracked conditions, while a higher sensitivity to this environmental condition seems to characterize the first cracking strength of the matrix. In the case of 150 and 500 cycles in Fig. 20a, the mechanical behavior is comparable to the 0 cycle case. This may be related to a self-healing phenomenon and late hydration of the pre-cracked specimens.

Fig. 21 shows two pictures of specimens treated with freezing–thawing cycles and then tested under tension. It is possible to see that, next to a crack developed in correspondence with a weft yarn, another crack forms and, H crack propagation can be observed on the edge (Fig. 21a): this behavior characterizes many un-cracked specimens. The development of the longitudinal crack at the middle of the speci-men thickness (Fig. 21b) may cause a detachment of the mortar cover and exposure of the fabric. It is worth noting that this detachment takes place at a stress level close to the maximum tensile strength (σ_{max}) and, therefore no delamination occurs at Serviceability Limit State ($\sigma_{SLS} \leq 0.4\sigma_{max}$).

To investigate the influence of thermal cycles on the material behav-ior, the variation according to cycle number of the main parameters that characterize the material response is shown in Fig. 22. In all the graphs,

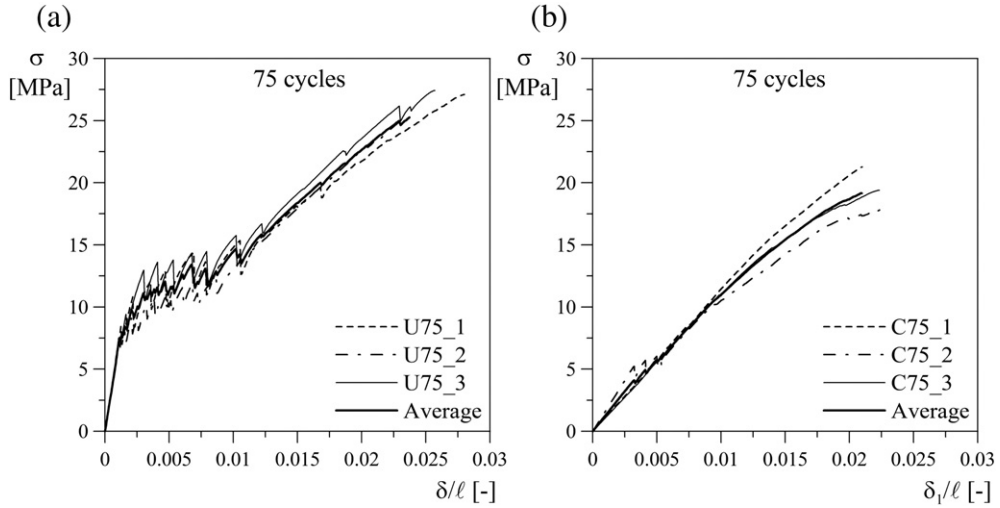

Fig. 15. Seventy-five cycles. Nominal stress vs. normalized displacement curves in uniaxial tension: un-cracked (a) and pre-cracked (b) specimens.

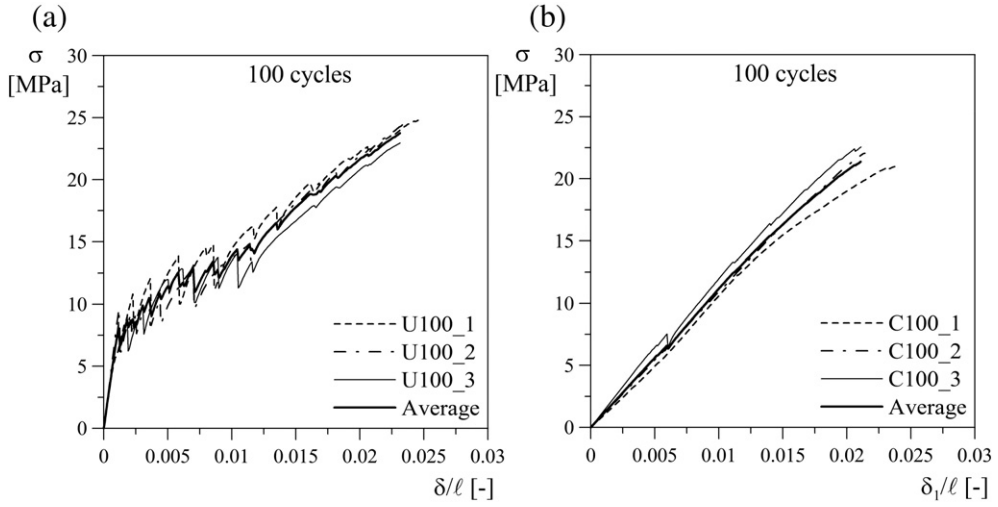

Fig. 16. One hundred cycles. Nominal stress vs. normalized displacement curves in uniaxial tension: un-cracked (a) and pre-cracked (b) specimens.

each marker represents the value assumed for each specimen by the considered parameter, normalized by the average value registered in the zero cycle case. The solid line connects the average value computed for the different number of cycles in the case of un-cracked specimens, and the dashed line refers to the pre-cracked condition.

Fig. 22a shows the trend of the maximum nominal stress registered for the different number of cycles. The negligible effect of the freezing–thawing cycles on the ultimate strength is confirmed here. For un-cracked specimens, a slight decrease in the maximum stress according to the increasing number of cycles is visible; however, even if 500 cycles are performed, 80% of the initial maximum nominal stress is still reached by the material. For pre-cracked specimens, the strength variation ranges between 0.8 and 1.2 without a clear trend. It is worth noting that the peak strength of each test has been normalized with respect to the peak strength obtained with the same clamping modalities at zero cycles and, therefore, pre-cracked specimens adopt a normalizing value that is 15% lower than the un-cracked specimens (0 cycle lines in Tables 4 and 5 respectively).

In Fig. 22b the relationship between the ultimate normalized displacement (registered when the maximum load is reached for each specimen) and number of freezing–thawing cycles is plotted. As in the previous graph, a trend of decreasing ultimate normalized displacement with an increasing number of cycles can be identified in un-cracked specimens, although for pre-cracked specimens this parameter does not seem to be affected by exposure to cycles. However, in both cases the values are all close to the normalized displacement measured for zero cycles (maximum average difference equal to 17%) also taking into account scattering of the results that, for this parameter, can reach 11%.

Fig. 22c shows the results in terms of first cracking strength versus number of cycles. Obviously these results are only available for un-cracked specimens, because the first cracking strength of pre-cracked specimens (collected in Table 5, column 10th) was reached before the exposure of specimens to thermal cycles. For a small number of cycles, up to 100, the first cracking strength does not seem to be affected by the freezing–thawing phenomenon (an enhancement of strength is even registered with respect to the 0 cycle condition), although exposure to a greater number of cycles causes a clear decrease in this property, as damage to the matrix is developing. It is important to point out that this parameter is characterized by a larger scattering than is the ultimate strength. This is in part due to the greater variability of the mortar's mechanical properties but, in particular, to the small eccen-tricities that may arise during the first phase of the test due to the mortar shrinkage, which causes a small curvature of the specimen. This curvature causes a misalignment of the load applied at the two ends of the specimen, which generates a bending moment on the specimen. The misalignment registered in all the experimental campaign is less than 3 mm and, for this reason, affects only the first cracking strength

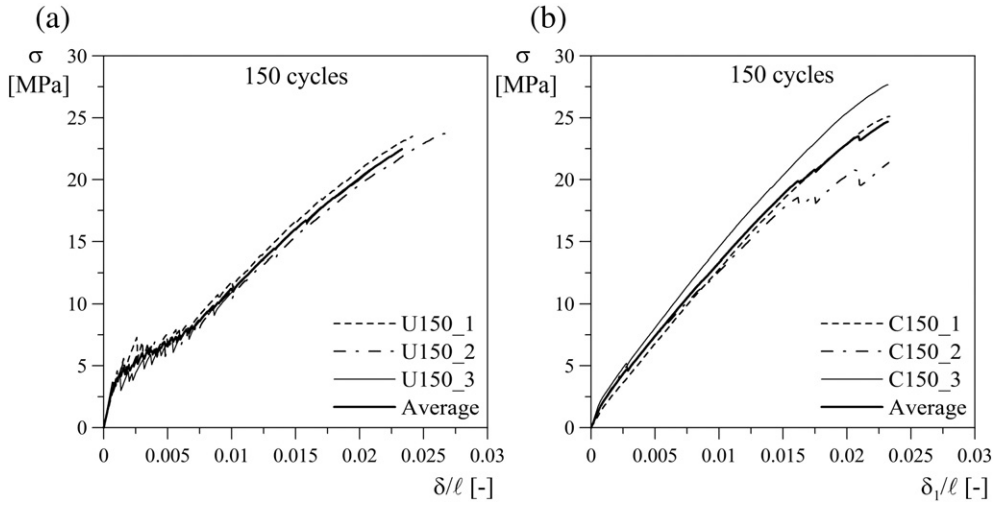

Fig. 17. One hundred fifty cycles. Nominal stress vs. normalized displacement curves in uniaxial tension: un-cracked (a) and pre-cracked (b) specimens.

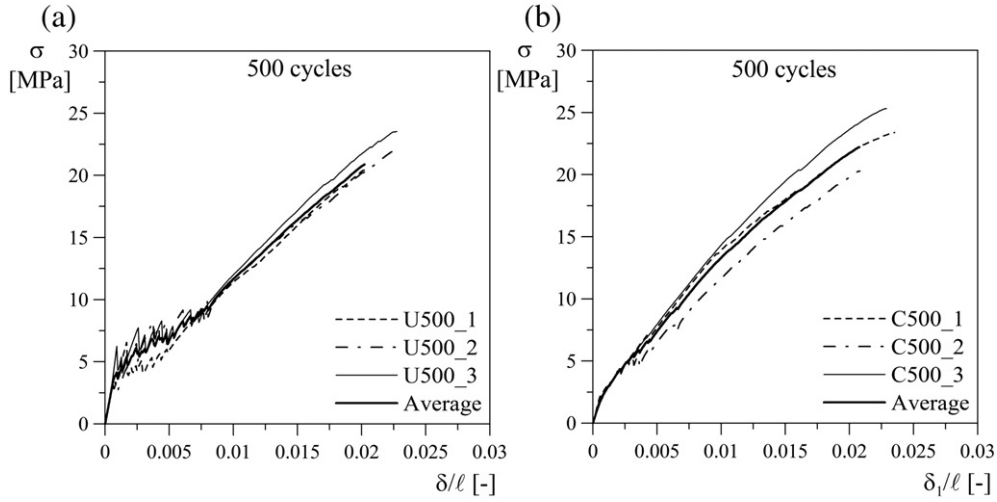

Fig. 18. Five hundred cycles. Nominal stress vs. normalized displacement curves in uniaxial tension: un-cracked (a) and pre-cracked (b) specimens.

without any significant impact on the cracked phase, also because of the formation of cracks that work as hinges at the specimen ends.

Considering the specimen mass variation, results in the literature suggest that conventional concrete specimens exhibit a mass reduction due to surface scaling, even if an air entraining agent is added to the mix: for a concrete characterized by a mean compressive strength of 40 MPa and a water to cement ratio equal to 0.45, Marzouk and Jiang [10] measured a mass loss, increasing with the number of cycles, of up to 2.2% (700 cycles) for 75 × 75 × 350 mm^3 specimens, and up to 5.5% (700 cycles) for thin specimens with the dimensions 20 × 75 × 300 mm^3. Shang and Yi [19] also registered a mass loss in-creasing with the number of cycles and with the decreasing of the class of concrete. In a high strength concrete characterized by a water to binder ratio equal to 0.3 and a mean compressive strength equal to 70 MPa, Marzouk and Jiang [10] found a smaller mass variation with re-spect to normal strength concrete (−0.6% for 75 × 75 × 350 mm^3 spec-imens and −0.5% for 20 × 75 × 300 mm^3 specimens, considering 700 cycles in both cases). For lower values of water to binder ratio, some cementitious particles in the hardened state of concrete remained unhydrated. Mass loss due to scaling is thus balanced by the water absorption, that leads to the hydration of un-hydrated cementitious particles and to the development of hydration products, resulting in a mass gain. Graybeal and Tanesi [14] observed this phenomenon when investigating the freezing–thawing durability of an ultra high perfor-mance concrete (UHPC), characterized by a water to cement ratio equal to 0.15. The phenomenon is enhanced in the case of specimens cured in air (such as those considered in this paper), because they exhibit lower levels of hydration when compared to UHPC cured in a wet environment. The later hydration can affect the mechanical properties of the material, limiting the reduction of strength due to freezing–thawing exposure.

Fig. 22d shows the percentage mass variation of the specimens with the increasing number of cycles. It is worth noting that all specimens ex-hibit a mass increase due to exposure to freezing–thawing cycles. The amount of this enhancement with an increasing number of cycles in-creases in uncracked specimens up to around 3.5% (registered for 150 and 500 cycles). In the case of pre-cracked specimens, the percentage variation of mass is higher than 5% for a low number of cycles (25, 50, 75 and 100), and decreases for 150 and 500 cycles.

In comparing the results discussed here with those presented elsewhere in the literature that exhibit a mass loss, it is important to point out that, contrary to the literature results, the specimens under discus-sion were not fully saturated when the cycles started. Even if the select-ed matrix is characterized by low water absorption (less than 3%), the water absorption measured on a TRC specimen (not thermally treated) 100 mm long, 70 mm wide and 6 mm thick reached an asymptote of about 5% after less than 1 week. This result indicates that fabric repre-sents a channel that favors water penetration inside the specimen since the fabric cross section is flush with the specimen short edges.

In the case of un-cracked specimens, the fabric is directly in contact with water only on the short sides, thus leading to very slow water pen-etration and consequently a very slow increase of mass with time for a fewer cycles than 100. For a higher number of cycles, micro-cracking due to the freezing–thawing cycles accelerates the water penetration,

Table 5
Tensile test results—pre-cracked (C) specimens.

		t [mm]	b [mm]	$\Delta m/m_i$ [%]	P_{max} [kN]	δ_{1u} [mm]	σ_{max} [MPa]	δ_{1u}/l [%]	σ_l [a] [MPa]	EF [−]
C0 (batch 7)	Average	6.2	70.3	–	10.05	5.94	23.15	2.22	4.52	0.91
	Scattering	3.3%	0.6%	–	9.2%	10.8%	6.5%	10.8%	9.1%	8.8%
C25 (batch 3)	Average	6.2	70.6	5.29	9.42	6.88	21.64	2.48	4.03	0.85
	Scattering	4.3%	1.3%	9.8%	3.5%	10.3%	1.9%	9.7%	5.2%	3.5%
C50 (batch 4)	Average	6.3	70.3	5.54	10.41	6.62	23.89	2.41	5.21	0.95
	Scattering	4.2%	0.9%	8.3%	9.1%	2.9%	8.7%	5.8%	11.5%	9.5%
C75 (batch 4)	Average	6.4	70.6	5.13	8.77	6.04	19.52	2.19	4.07	0.80
	Scattering	3.1%	0.4%	7.8%	8.2%	4.8%	9.0%	4.1%	16.2%	8.8%
C100 (batch 4)	Average	6.0	70.7	5.88	9.23	6.07	21.86	2.21	4.35	0.84
	Scattering	1.7%	1.3%	34.4%	6.2%	7.2%	3.9%	8.1%	18.9%	6.0%
C150 (batch 3)	Average	5.7	70.4	0.80	9.94	6.37	24.71	2.32	4.36	0.90
	Scattering	5.3%	0.7%	148.8%	10.3%	0.6%	13.6%	0.4%	1.6%	10.0%
C500 (batch 3)	Average	5.8	70.6	3.99	9.43	6.16	22.99	2.24	3.66	0.86
	Scattering	5.2%	1.1%	18.5%	6.4%	7.1%	11.8%	7.1%	19.9%	7.0%

[a] Values obtained in the pre-cracking phase (soft clamp) before thermal cycles.

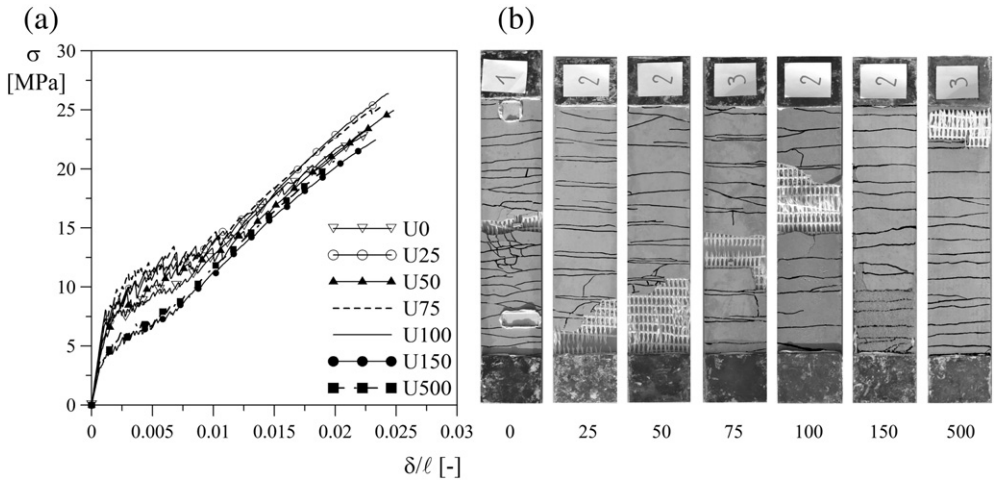

Fig. 19. Average nominal stress vs. normalized displacement curves after a different number of cycles (a) and corresponding crack patterns (b) for un-cracked specimens.

as can be observed by the increase of the curve slope between 100 and 150 cycles. The final plateau can be related to full saturation of the specimen, and the lower value of this plateau with respect to the 5% asymptote previously discussed may be due to the scaling phenomenon observed in the case of 150 and 500 cycles, which caused a mass loss.

Conversely, in pre-cracked specimens the initial cracks increase the fabric surface that is directly in contact with water, thus leading to a very fast increase in the mass (about 5.5%) since the 25 cycles situation (that corresponds to 5 days' permanence into the water). It is worth noting that the crack spacing due to pre-cracking is comparable with the length of the specimen used for water absorption measurements,

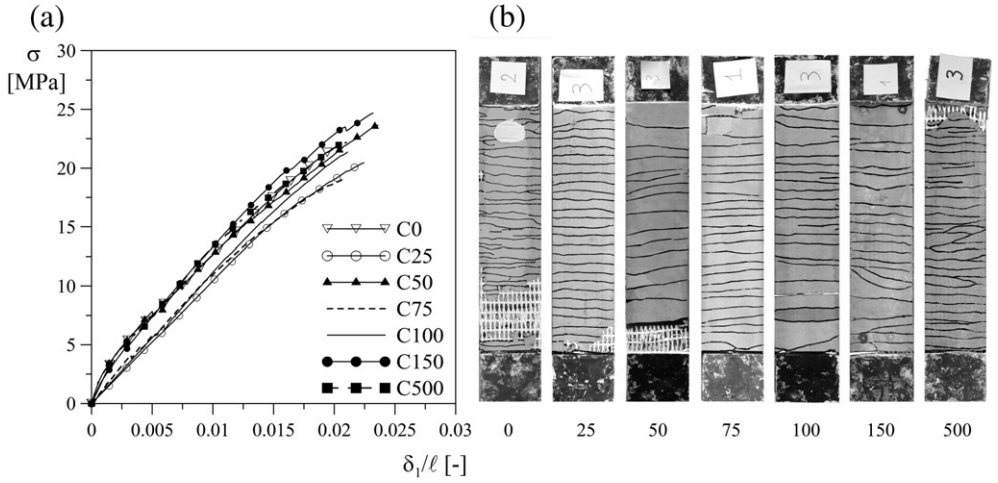

Fig. 20. Average nominal stress vs. normalized displacement curves after a different number of cycles (a) and corresponding crack patterns (b) for pre-cracked specimens.

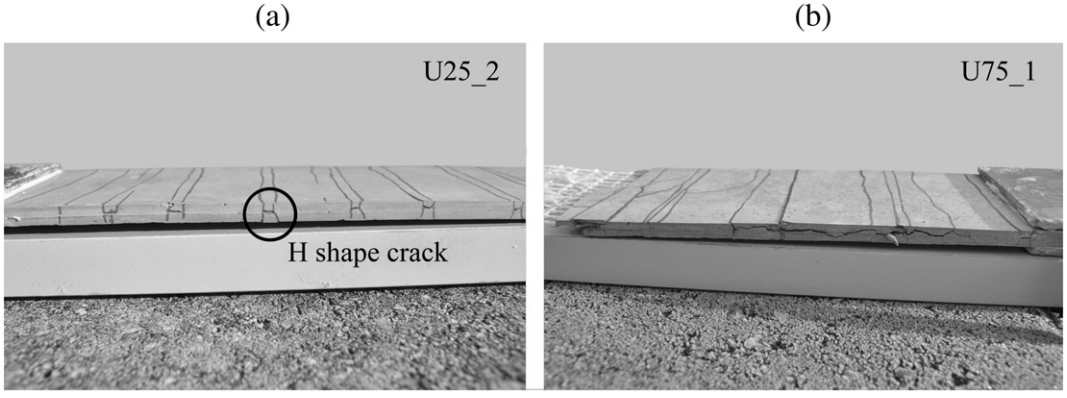

Fig. 21. Specimens after tensile test: H crack propagation (a) and development of a longitudinal crack at the middle of the specimen thickness (b).

thus confirming the speed of the water penetration process. The sudden decrease of the mass observed from 150 cycles must be related to the previously discussed scaling phenomenon. The final increase of the mass may be driven, as discussed by Graybeal and Tanesi [14], by a late hydration.

Fig. 22e shows the trend of the efficiency factor (EF) with the cycle number growth. This factor is a measure of the effectiveness of the fabric–matrix bond: a value larger than one indicates a positive interaction between the mortar and its reinforcement, while values lower than one mean a bond weakness: the lower the value the higher this weakness. Looking at the graph, it is clear that, although the un-cracked specimens behave better than pre-cracked ones for a low number of cycles, for a high number of cycles the EF tends to converge on the value of 0.8.

The evolution, with the number of cycles, of three stiffness coefficients (k_1, k_2 and k_3) is plotted in Fig. 22f. These coefficients are defined in Fig. 6a and b and their average values are collected in Table 6, togeth-er with the scatterings. k_1 represents the initial stiffness of the compos-ite material in the un-cracked condition (thus specimens are tested from the beginning with the hard clamping system); it is computed as the slope of the nominal stress vs. normalized displacement curve be-tween zero and $0.1\sigma_{max}$. This parameter is just a measure of the initial stiffness of the composite and it is computed to compare specimens

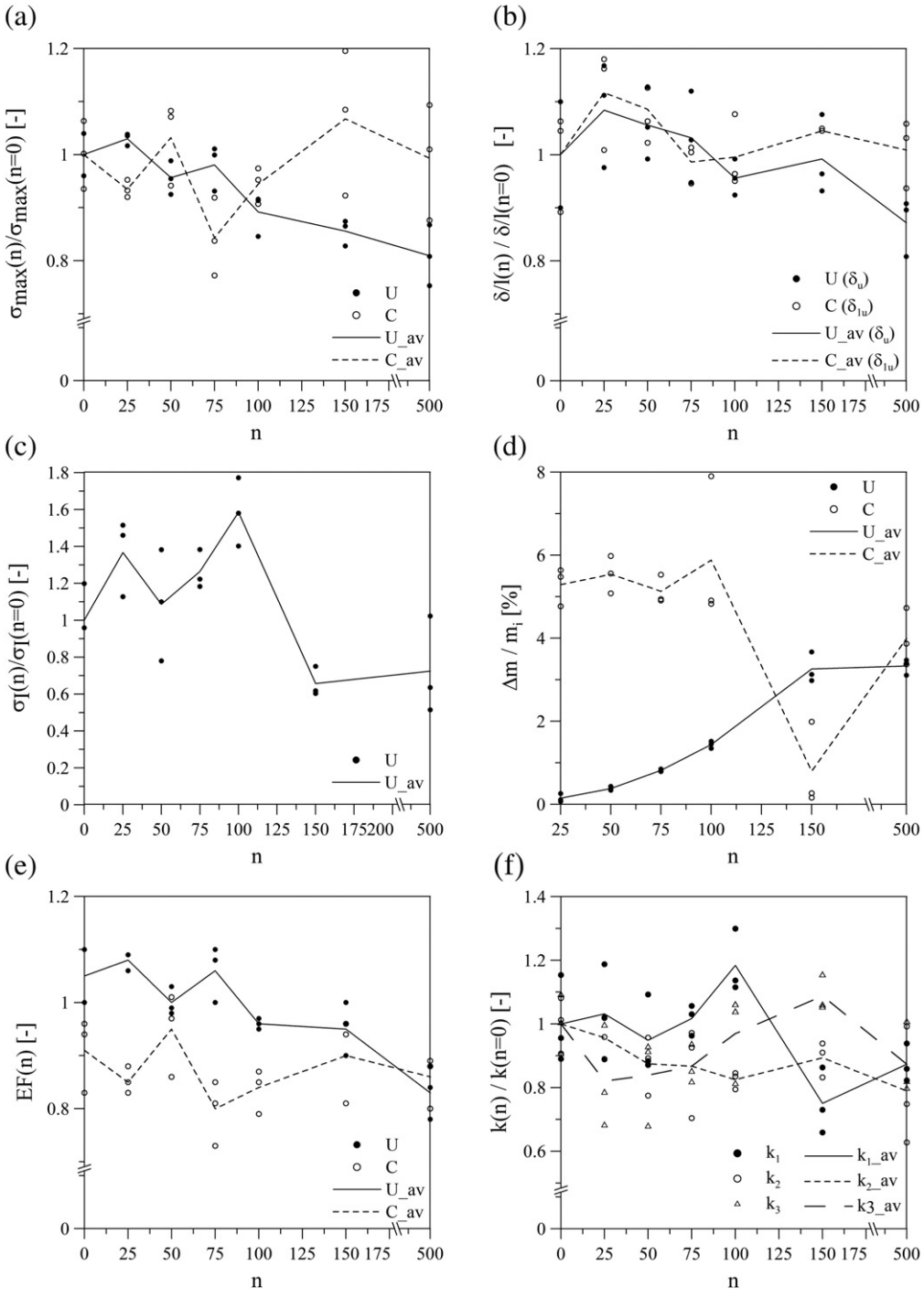

Fig. 22. Test results: (a) peak strength vs. number of cycles, (b) peak normalized displacement vs. number of cycles, (c) first cracking strength vs. number of cycles, (d) mass variation vs. number of cycles, (e) EF vs. number of cycles and (f) specimen stiffness vs. number of cycles.

Table 6
Tensile test results—measured values of k_1, k_2 and k_3.

		k_1 [MPa]	k_2 [MPa]			k_3 [MPa]
U0	Average	6287.55	1000.01	C0	Average	953.04
	Scattering	15.4%	9.3%		Scattering	9.4%
U25	Average	6486.73	956.34	C25	Average	781.98
	Scattering	15.1%	7.0%		Scattering	21.3%
U50	Average	5967.44	874.77	C50	Average	799.61
	Scattering	15.1%	11.4%		Scattering	19.2%
U75	Average	6393.08	867.25	C75	Average	826.61
	Scattering	5.3%	18.8%		Scattering	7.8%
U100	Average	7442.38	825.15	U100	Average	924.24
	Scattering	9.8%	3.7%		Scattering	16.3%
U150	Average	4720.73	893.51	C150	Average	1036.86
	Scattering	14.9%	6.9%		Scattering	6.0%
U500	Average	5492.86	789.51	C500	Average	832.77
	Scattering	7.5%	25.6%		Scattering	15.2%

treated with a different number of cycles; it does not correspond to the Young's modulus of the cementitious matrix, as the normalized displacement is taken into account instead of the strain (thus including the sliding between the specimen and the clamping devices). Parameter k_2 is also computed for the un-cracked condition. This coefficient is obtained as the slope of the final branch of the nominal stress vs. normalized displacement curve of TRC in tension. In this branch, only the contribution of the fabric is noticeable and no further cracks appear in the matrix. In this case 0.7 σ_{max} and 0.8 σ_{max} are assumed as limit values. Finally, k_3 is computed as k_2, but referring to pre-cracked specimens.

The evolution of the initial stiffness (k_1) is mainly related to the damage caused by the thermal cycles to the mortar matrix and it is possible to see that it is similar to that experienced by the first cracking strength. This is due to the fact that both parameters are governed by the same damage of the matrix, but also that they have the same sensitivity to the test scheme eccentricity. In any case, it is clear from the results that small damage values (a stiffness reduction lower than 20%) are available in the mortar matrix.

The evolution of the post-cracking stiffness parameters (k_2 and k_3) represents the damage caused in both the fabric itself and the mortar-fabric interface. It is worth noting that, in the case of pristine material (0 cycles), the stiffness in the cracked phase (k_2 and k_3) is barely affected by the test modalities, showing a maximum average difference lower than 5%.

These parameters, in addition to those already discussed, confirm the low sensitivity of the TRC to freezing–thawing cycles.

5. Conclusions

The experimental results discussed in this paper allow conclusions to be drawn about the behavior of the TRC investigated when exposed to freezing–thawing cycles.

In particular, two different phenomena seem to govern the behavior of the material: the damage due to thermal cycles, and the matrix self-healing and late hydration due to the permanence in water of the material. Thanks to the presence of cracks during the thermal cycles, and therefore an easier penetration of water, self-healing and a late hydration effect mainly appear in pre-cracked (C) situations. The larger water absorption of pre-cracked specimens, which is directly related to the self-healing, is also clearly visible in the mass growth (Fig. 22d).

These considerations can be supported by the following evidence:

1) a thermal cycle number larger than 100 causes a degradation of the cement matrix, as can be clearly observed looking at the first cracking strength of the un-cracked (U) specimens tested, which experienced up to a 40% reduction with an increasing number of cycles (Fig. 22c);
2) in the case of un-cracked (U) specimens, thermal cycles also affect the ultimate tensile strength (σ_{max}) and therefore the efficiency factor (EF) of the material (Fig. 22a and e) may be due to a degradation of the bond strength of the cement matrix. Because of the brittleness of the reinforcement, the tension stiffening phenomenon influences the efficiency factor, the maximum tensile strength and the corresponding displacement (δ_u); in fact the failure is governed by bond, which controls the energy release rate;
3) in the case of pre-cracked (C) specimens, an initial maximum strength decay is recovered for a cycle number larger than 75 (Fig. 22a). This phenomenon can be related to a larger permanence in water and, therefore, to a possible activation of self-healing and late hydration that may lead to a bond strength recovery;
4) bond strength recovery can also be observed in the denser crack pattern of pre-cracked specimens (Fig. 20b), with a crack distance equal to the weft spacing for all the cycle numbers considered. Further consequences of the bond strength recovery, due to self-healing and late hydration of pre-cracked specimens, can be observed in the increasing initial stiffness with the increased cycle number (Fig. 20a) and in the recovery of stiffness (k_3, Fig. 22f) after 75 cycles in the cracked phase.

Acknowledgments

The authors would like to thank Gavazzi company for supplying the AR glass fabrics. The research was financially supported by the European "EASEE" project, Grant Agreement No. 285540, Thematic Priority: EeB.NMP.2011-3—Energy saving technologies for buildings envelope retrofitting, Starting date of project: 1st March, 2012, Duration: 48 months.

References

[1] M. Butler, V. Mechtcherine, S. Hempel, Durability of textile reinforced concrete made with AR glass fibre: effect of the matrix composition, Mater. Struct./Mater. Constr. 43 (2010) 1351–1368.
[2] M. Horstmann, J. Hegger, M. Zell, C. Kulas, Large-sized building envelopes and slen-der shell structures made of TRC, Proceedings of the 8th International Symposium on Utilization of High-Strength and High-Performance Concrete, Tokyo, 2008, pp. 1183–1190.
[3] M. Curbach, S. Sheerer, Concrete light—Possibilities and Visions, Proceedings of the fib Symposium Prague 2011 - Concrete Engineering for Excellence and Efficiency, 2011, pp. 29–44.
[4] J. Orlowsky, M. Raupach, Durability model for AR-glass fibres in textile reinforced concrete, Mater. Struct./Mater.Constr. 41 (2008) 1225–1233.
[5] P. Purnell, J. Beddows, Durability and simulated ageing of new matrix glass fibre reinforced concrete, Cem. Concr. Compos. 27 (2005) 875–884.
[6] ASTM, International C666/C 666<ce:hsp sp="0.25"/>M–03 Standard Test Method for Resistance of Concrete to Rapid Freezing and Thawing, 2008.
[7] A. Neville, Properties of Concrete, Wiley, New York, 1996.
[8] G. Lomboy, K. Wang, Effects of strength, permeability, and air void parameters on freezing–thawing resistance of concrete with and without air entrainment,
J. ASTM Int. 6 (2009).
[9] W. Sun, Y. Zhang, H. Yan, R. Mu, Damage and damage resistance of high strength concrete under the action of load and freeze-thaw cycles, Cem. Concr. Res. 29 (1999) 1519–1523.
[10] H. Marzouk, D. Jiang, Effects of freezing and thawing on the tension properties of high-strength concrete, ACI Mater. J. 91 (1994) 577–586.
[11] P. Aïtcin, The durability characteristics of high performance concrete: a review, Cem. Concr. Compos. 25 (2003) 409–420.
[12] K. Wang, G. Lomboy, R. Steffes, Investigation into Freezing–Thawing Durability of Low-Permeability Concrete with and without Air Entraining Agent, National Concrete Pavement Technology Center - Institute for Transportation - Iowa State University, 2009.
[13] Canadian Standard Association, CSA A23.1 – Concrete materials and methods of concrete construction / Test methods and standard practices for concrete, 2009.
[14] B. Graybeal, J. Tanesi, Durability of an ultrahigh-performance concrete, J. Mater. Civ. Eng. 19 (2007) 848–854.
[15] A. Çavdar, Investigation of freeze–thaw effects on mechanical properties of fiber reinforced cement mortars, Compos. Part B 58 (2014) 463–472.

[16] European Standard EN 196–1, Method of Testing Cement—Part 1: Determination of Strength, 2005.
[17] I.G. Colombo, A. Magri, G. Zani, M. Colombo, M. di Prisco, Erratum to: textile reinforced concrete: experimental investigation on design parameters, Mater. Struct./Mater. Constr. (2013) 1–19.
[18] J. Hartig, F. Jesse, K. Schicktanz, U. Häußler-Combe, Influence of experimental setups on the apparent uniaxial tensile load-bearing capacity of Textile Reinforced Concrete specimens, Mater. Struct./Mater. Constr. 45 (2012) 433–446.
[19] H.S. Shang, T.H. Yi, Freeze-thaw durability of air-entrained concrete, Sci. World J. vol.(2013) 6, http://dx.doi.org/10.1155/2013/650791.